CHEMISTRY OF MATERIALS

Article

pubs.acs.org/cm

High Performance, Low Temperature Solution-Processed Barium and Strontium Doped Oxide Thin Film Transistors

Kulbinder K. Banger,[†,⊥] Rebecca L. Peterson,[†,∥,⊥] Kiyotaka Mori,[‡,⊥] Yoshihisa Yamashita,[‡,⊥] Timothy Leedham,[§] and Henning Sirringhaus*[,†]

[†]Cavendish Laboratory, Department of Physics, University of Cambridge, Cambridge CB3 0HE, United Kingdom

[‡]Panasonic Corporation, Osaka 571-8501, Japan

[§]Multivalent Ltd., Eriswell, Suffolk IP27 9BJ, United Kingdom

Supporting Information

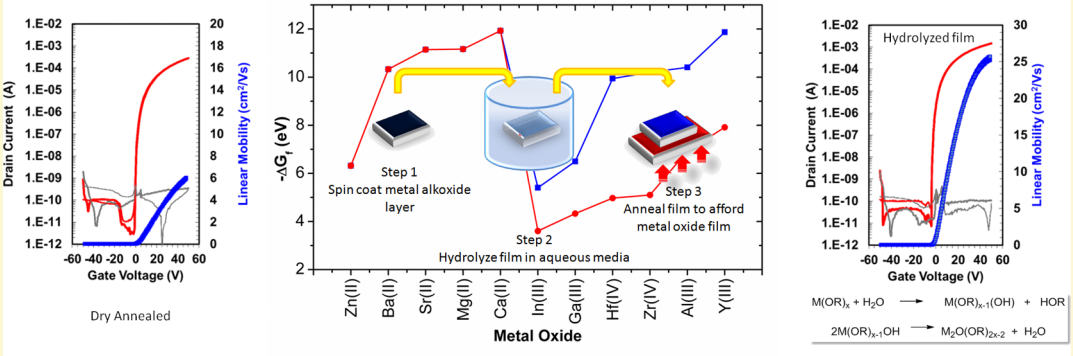

ABSTRACT: Amorphous mixed metal oxides are emerging as high performance semiconductors for thin film transistor (TFT) applications, with indium gallium zinc oxide, InGaZnO (IGZO), being one of the most widely studied and best performing systems. Here, we investigate alkaline earth (barium or strontium) doped InBa(Sr)ZnO as alternative, semiconducting channel layers and compare their performance of the electrical stress stability with IGZO. In films fabricated by solution-processing from metal alkoxide precursors and annealed to 450 °C we achieve high field-effect electron mobility up to 26 $cm^2 V^{-1} s^{-1}$. We show that it is possible to solution-process these materials at low process temperature (225−200 °C yielding mobilities up to 4.4 $cm^2 V^{-1} s^{-1}$) and demonstrate a facile "ink-on-demand" process for these materials which utilizes the alcoholysis reaction of alkyl metal precursors to negate the need for complex synthesis and purification protocols. Electrical bias stress measurements which can serve as a figure of merit for performance stability for a TFT device reveal Sr- and Ba-doped semiconductors to exhibit enhanced electrical stability and reduced threshold voltage shift compared to IGZO irrespective of the process temperature and preparation method. This enhancement in stability can be attributed to the higher Gibbs energy of oxidation of barium and strontium compared to gallium.

1. INTRODUCTION

Mixed metal oxides are the subject of intense research efforts due to their relative ease of processing and high performance in a range of electronic and optoelectronic devices.[1−5] A major research and development focus has been on the transparent conducting oxide (TCO) alternatives to indium tin oxide[3,4] and semiconducting materials for thin film transistor (TFT) alternatives to amorphous/polycrystalline silicon.[1,2,5] Although most work on mixed metal oxides has focused on vacuum-based deposition processes, such as sputtering,[6] solution processing has emerged as a viable alternative that produces materials of comparable device performance and stability.[7,8] Amorphous indium gallium zinc oxide (IGZO) is currently a leading candidate for replacing amorphous silicon in the next generation of TFT for active matrix display addressing.[1−6] This can be attributed to its innate high carrier mobility, excellent operational stability, and optical transparency which enable new types of displays such as transparent or ultrahigh resolution liquid crystal displays (LCDs) or organic light-emitting diode (OLED) displays.[1,2,5,9,10]

We have recently developed a powerful solution processing approach to amorphous mixed metal oxides based on sol−gel processing from metal alkoxide precursors and have demonstrated solution-processed IGZO TFTs prepared at low process temperature (230−275 °C) with performance and operational stress stability comparable to that of sputtered devices.[11] One of the strengths of the approach is that it provides versatile access to a wide range of elemental compositions, hence new semiconductors. Doping of mixed metal oxides by are variety of elements, including alkaline earths,[12−14] rare earth,[15,16] and main group,[17−19] as well as transition metals,[17,18,20−26] has been

Received: October 29, 2013
Published: December 22, 2013

   dx.doi.org/10.1021/cm4035837 | Chem. Mater. 2014, 26, 1195−1203

reported previously. A very important figure of merit for these mixed metal oxide semiconductors is the electronic stability of the material, which in turn equates to a lifetime of the TFT device. However, no evidence was found for these dopants providing advantages in either device performance or electrical stability over conventional Ga doping.[27]

We have also been investigating the development of new oxide semiconductors and the use of different chemical routes for solution-processed oxides for several years, namely, Ba and Sr alkaline earth doping,[28] and we also note recent published work by Kim et al.;[12,13] however, semiconductor device performance was limited. Building on the platform of alkoxide molecular precursor chemistry, we now demonstrate here for the first time that low-temperature, solution-processed InSrZnO (ISZO) and InBaZnO (IBZO) do indeed offer comparable and, in some respects, superior performance to IGZO with excellent control of carrier concentration, TFT device performance, and operational stability.

We also investigate the role of impurities in these materials by investigating high purity precursors synthesized by alcoholysis reaction of alkyl metal starting reagents as opposed to the standard route based on metal halide starting reagents.

2. EXPERIMENTAL SECTION

Materials/Synthesis. Indium isopropoxide cluster ($In_5O(OCH(CH_3)_2)_{13}$) (**1**), zinc *bis*-methoxyethoxide ($Zn(OCH_2CH_2OCH_3)_2$) (**2**), and ($Ga(OCH(CH_3)_2)_3$) (**3**) coordination derivatives were obtained from Multivalent Ltd. (Eriswell, U.K.) as 0.1 M parent alcohol solutions and used as received.

Indium, zinc, strontium, and barium organometallic complexes are synthesized via the "ink-on-demand" processes as briefly described below, with detailed characterization included in Supporting Information and designated references.

*[EtZnOCH(CH$_3$)$_2$] (**4**).* Under anaerobic conditions, diethyl zinc (0.1 mL, 1.0 M, Aldrich, U.K.), is added to anhydrous propanol-2-ol, (0.9 mL, ROMIL, U.K.), dropwise, in a 4 mL glass vial which results in effervescence through elimination of ethane gas. The transparent, colorless zinc alkoxide solution is agitated briefly and then used as is or diluted further to the desired molarity.

*[Me$_{3-n}$In(OR)$_n$] (**5**, **6**).* Under anaerobic conditions, trimethylindium (0.25 g, 1.56 mmol), (Hitech, Aldrich, U.K.) is dissolved in anhydrous toluene (Romil, U.K.) to afford a 1.0 M stock solution. A total of 0.4 mL of this clear transparent stock solution is then added to 3.6 mL of the anhydrous alcohol, R = OC_4H_9 (**5**), $OCH(CH_3)_2$ (**6**), dropwise in a 4 mL glass vial which results in effervescence with elimination of methane gas. The transparent colorless indium alkoxide solution is then agitated and used as is or diluted to the desired molarity.

*[Ba(OCH(CH$_3$)$_2$)$_2$] (**7**).* Under anaerobic conditions, barium metal pieces (less than 0.50 g, Aldrich) are washed with hexane and then cleaved to reveal fresh unoxidized surfaces. The freshly cut barium is then diced and weighed in a nitrogen atmosphere and slowly added to the desired amount of anhydrous propan-2-ol (ROMIL, UK) to achieve a 0.1 M solution. The reaction proceeds smoothly with effervescence and is left overnight with stirring. Once the reaction is complete the solution is then filtered through a graded PTFE high particulate filter (10−0.2 μm, Millipore) to afford a colorless transparent solution.

*[Sr(OCH(CH$_3$)$_2$)$_2$] (**8**).* **8** is made under equivalent conditions as described for **7** above or can be purchased from Multivalent Ltd., U.K.

*[(MeIn)$_5$O(OR)$_8$] (**9**−**11**).* The methyl indium organometallic cluster cage compounds are made according to the published work as first described by Muller et al.,[29] using standard Schlenk techniques. Briefly, under anaerobic conditions, trimethylindium (0.54 g, 3.37 mmol, Hitech, Aldrich, U.K.) is dissolved in 1 mL of anhydrous toluene (Romil, U.K.). This is then added dropwise to a 100 mL predried Schlenk flask charged with 30 mL of anhydrous parent alcohol under N_2 to achieve the "simple" methyl indium organometallic compound as described above. This is then refluxed under nitrogen for 4 h affording a clear colorless solution of the cluster cage derivative [$(MeIn)_5O(OR)_8$] (where R = OC_4H_9 (**9**), $OCH(CH_3)_2$ (**10**), and methoxyisopropoxide (OMIP) $C_4H_{10}O_2$ (**11**)). The transparent colorless indium alkoxide solution is then used as is or diluted with the same parent alcohol to obtain the desired molarity.

TFT Fabrication. Transparent, colorless indium zinc oxide (IZO) "ink" is prepared under anaerobic conditions by blending 0.1 M solution of the In and Zn solutions in at least a 7:3 metal oxide (In to Zn) ratio. The ink is then stirred and used as is. In order to obtain Ba- or Sr-doped inks (IBZO & ISZO), an indium zinc oxide ink (7:3 molar oxide ratio) is first prepared. The designated alkaline earth doping level is then blended to achieve clear inks of 5−20% Ba or Sr composition. Solution processed IZO and doped oxide TFTs are prepared on heavily doped silicon substrates with thermal SiO_2 gate dielectric (100 nm), or Al_2O_3 (55 nm), deposited via atomic layer deposition at 180 °C. Substrates were cleaned by solvent cleaning, drying, and oxygen plasma treatment. Films were fabricated by spin coating under an inert, nitrogen atmosphere using a maximum spin speed of 4000 rpm and a spin time of 60 s. Samples were then either used as-is or subjected to a brief heating cycle at 200 °C for 5 min before removal to air, where they were annealed at 450 °C unless otherwise stated. In the case of in situ UV air annealing, as-spun samples were placed directly on a hot plate held at 200−225 °C and exposed to UV254 nm 5−8 mW/cm^2 using a hand-held Lab UV lamp in air (UVP Cambridge Inc.), during the course of annealing.

A thermocouple probe was mounted directly on the silicon substrates which confirmed that the maximum process temperature was ±3 °C of the set point anneal temperature. In addition, a second thermocouple probe was placed 10 mm above the coated wafers where a maximum headspace temp of 151 °C was noted when processed at 200 °C. Tungsten contacts of <100 nm thickness were sputtered through a shadow mask to form source and drain electrodes in a bottom-gate, top-contact (BGTC) thin film transistor. The transistors were either left as-is or, if encapsulated, a fluoropolymer was spin coated over both source/drain and channel before been isolated by mechanical scribing or wet chemical etching.

Device Characteristics. Device characteristics were measured using an Agilent 4156C and 4155 Semiconductor Parameter Analyzer. Measurements were typically made in continuous mode, at source drain voltage (V_{DS}) of 1 or 5 V. Stress bias measurements were made at either room temperature with a constant current bias or constant voltage as indicated. During the current stress the voltage applied to the gate was shorted to that applied to the drain, and this voltage was adjusted to achieve the required current stress setting. At regular intervals during the stress, the stress was temporarily removed in order to record transfer characteristics to monitor the degree of threshold voltage shift. The field-effect mobility in the linear operation regime was extracted as a function of gate voltage using eq 1.

$$\mu_{eff} = (\partial I_D/\partial V_{GS})((W/L)C_{ox}V_{DS})^{-1} \quad (1)$$

where I_D is the measured drain current, W/L is the channel width/length, respectively, and C_{ox} is the capacitance of the gate dielectric. Mobility values quoted in the text are maximum mobilities extracted at a gate voltage as shown in transfer curves. The threshold voltage, used to measure stress bias shifts, was also obtained from the linear I_D-V_{GS} curve. The subthreshold slope, S (V/dec), was taken as the minimum value of the inverse slope of the $\log_{10}(I_D)$ vs V_{GS} characteristics. The turn-on voltage was defined as the voltage at which the minimum subthreshold slope occurs. The ON/OFF ratio is defined as the maximum I_D divided by the I_D 5 V below turn-on. Hysteresis is taken to be the difference between the interpolated gate voltages at 10 nA drain current for the forward and reverse I_D-V_{GS} traces.

3. RESULTS AND DISCUSSION

Ba and Sr metals were preferential chosen as suitable candidates to dope IZO based on the calculation of the Gibbs energy of oxidation for a variety of dopants candidates as shown in Figure 1 and their larger cation radii (Table 1, Supporting

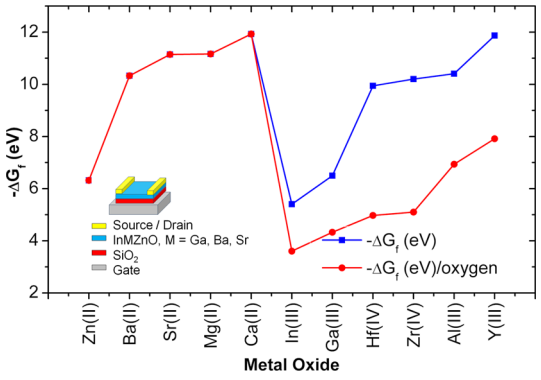

Figure 1. Gibbs Energy of oxidation calculated for selected metals. Inset shows BGTC and TFT architecture used to compare different metal doped InZnO semiconducting channel layers.

Information). Thus, replacement of Ga for the tighter oxygen binding alkaline earth metals is thought to suppress the formation of excess charge carriers in the oxide film leading to negative transistor turn-on voltages or unwanted deep oxygen trap states, which may impede charge transport and hence reduce device mobility.[30] Additionally, Ba and Sr have larger cation radii then In and Zn, which can impart sufficient disorder within the IZO framework to promote the desirable formation of an amorphous phase.[31] To validate the use of Ba- and Sr-doped IZO oxide as semiconducting channel layers for thin film transistors, solution processed IBZO and ISZO were first fabricated using a relatively high temperature (450 °C) annealing process as reference. We will discuss below films processed at lower and more practically relevant annealing temperatures. Alcohol-based 0.1 M solutions of the individual alkoxide precursors for indium (**1**), zinc (**2**), and barium (**7**) or strontium (**8**) are blended with a 7:3 In:Zn oxide ratio. Figure 2 shows typical transfer and output characteristics of IBZO and ISZO TFTs with increasing percentage of BaO and SrO doping, respectively. Devices fabricated using these layers demonstrate excellent TFT characteristics with tightly controlled turn-on voltage around 0 V, high ON/OFF ratios (10^7–10^8), and high carrier mobilities (Table 2, Supporting Information). For both dopants we observe a monotonic decrease of mobility with increasing concentration of BaO or SrO, from values on the order of 10–12 $cm^2\ V^{-1}\ s^{-1}$ for 5% doping to 6–7 $cm^2\ V^{-1}\ s^{-1}$ for 15% doping. This is presumably a reflection of higher structural disorder with increasing doping concentration. Similar devices made at reduced temperatures (350 °C) also exhibit very good device performance with mobilities on the order of 4 $cm^2\ V^{-1}\ s^{-1}$ (Figure S1, Supporting Information).

One of the notable features of metal alkoxide molecular precursors is the large difference in the Pauli electronegativity in the M-OR bond, which renders the molecular alkoxide susceptible to hydrolysis through nucleophilic attack, eq 2.[32,33] This chemical reactivity can be exploited when thin film alkoxide coatings are exposed to an aqueous medium promoting the conversion of the alkoxide coating to an extended −M−O−M− film network.[33,34]

$$M(OR)_x + H_2O \rightarrow M(OR)_{x-1}(OH) + HOR$$
$$2M(OR)_{x-1}OH \rightarrow M_2O(OR)_{2x-2} + H_2O \quad (2)$$

where M = metal and R = organic ligand.

This is clearly demonstrated when comparing ISZO and IBZO TFTs made in the absence of exposure to water (Figure 2), with those fabricated where the spin-coated alkoxide layers are dipped in deionized water (approximately 10 MΩ) for 10 s prior to air annealing, Figure 3 and Figure S2 (Supporting Information). TFTs made from thin films subjected to this mediated hydrolysis prior to air annealing show at least a two- to threefold enhancement in mobility to approximately 18 $cm^2\ V^{-1}\ s^{-1}$ for IBZO and 25 $cm^2\ V^{-1}\ s^{-1}$ for ISZO, respectively. Statistical data analysis for IBZO 49 TFT's shows devices with an average field effect mobility of 17.18 $cm^2\ V^{-1}\ s^{-1}$ (σ = 1.7), Figure 3c. But importantly, minimum variation in other key TFT parameters such as turn-on (V_{on}) and threshold (V_{th}) voltage and hysteresis between forward and reverse current–voltage sweeps is also found.

The rate constants for H_2O substitution for Ba and Sr moieties (10^9–10^{10} $k^{Ba,Sr}$, s^{-1}) are several orders of magnitude higher in comparison to those of zinc (10^7 k^{Zn}, s^{-1}) and trivalent indium and gallium at 10^2 (k^{In}, s^{-1}) and less than 10^1 (k^{Ga}, s^{-1}), respectively. Thus, Ba and Sr alkoxides hydrolyze faster upon exposure to water than the other alkoxide components.[32,35] This in turn enhances the olation condensation mechanism since the aqua or alcohol moieties are good leaving groups.[36] To see the effect of this on the fully formed oxide films, analysis of atomic composition of the two samples was undertaken by XPS (Figure S3, Supporting Information).

Due to the expected preferential dissolution of the alkaline earth precursors in water there is a reduction in Ba/Sr oxide doping from approximately 15% to 5% upon dipping the films in water, which is in part responsible for the increase in mobility from 6 to 7 $cm^2\ V^{-1}\ s^{-1}$ to 17–25 $cm^2\ V^{-1}\ s^{-1}$. Direct comparison of similar IBZO or ISZO devices with 5% alkaline earth oxide doping annealed without dipping in water shows intermediate mobilities of approximately 10–12 $cm^2\ V^{-1}\ s^{-1}$ (Figure 3). Thus it is clear that while the reduction in doping concentration from 15 to 5% makes some contribution toward enhancing device mobility, there must be a second beneficial effect on mobility from the process of dipping the films into water, promoting metal oxide film formation.[33,37,38]

Performing the processing in the presence of water also provides a route to lower annealing temperatures. Films dipped in water for 5–10 s before annealing in air exhibited high TFT performance with mobility of approximately 2–4 $cm^2\ V^{-1}\ s^{-1}$ for annealing temperatures of 275–300 °C (Figure 4 and Figure S4, Supporting Information, for IBZO). Devices were also made at 275 °C through in situ wet annealing in a humid atmosphere for approximately 5 min, followed by dry air annealing on a second hot plate preheated at 275 °C as previously reported.[11] TFTs processed in this way exhibited mobilities around 5 $cm^2\ V^{-1}\ s^{-1}$ (Figure S5, Supporting Information), comparable to those of films dipped in water. The slighter higher mobilities suggest that in situ hydrolysis provides better control of the defect density in the films compared to the water dipping method.

In our previous work on IZO and IGZO we have observed by XPS and atomic absorption spectroscopy the presence of residual alkaline earth metal as well as halide impurities in the oxide channel layer. These are introduced during the preparation of the precursors from the metathesis reaction between $Ba(OR)_2$ and $InCl_3$ during the synthesis (**1**).[11,39] This means that in the experiments discussed above there is always a small background concentration, as recorded by XPS analysis,

dx.doi.org/10.1021/cm4035837 | Chem. Mater. 2014, 26, 1195–1203

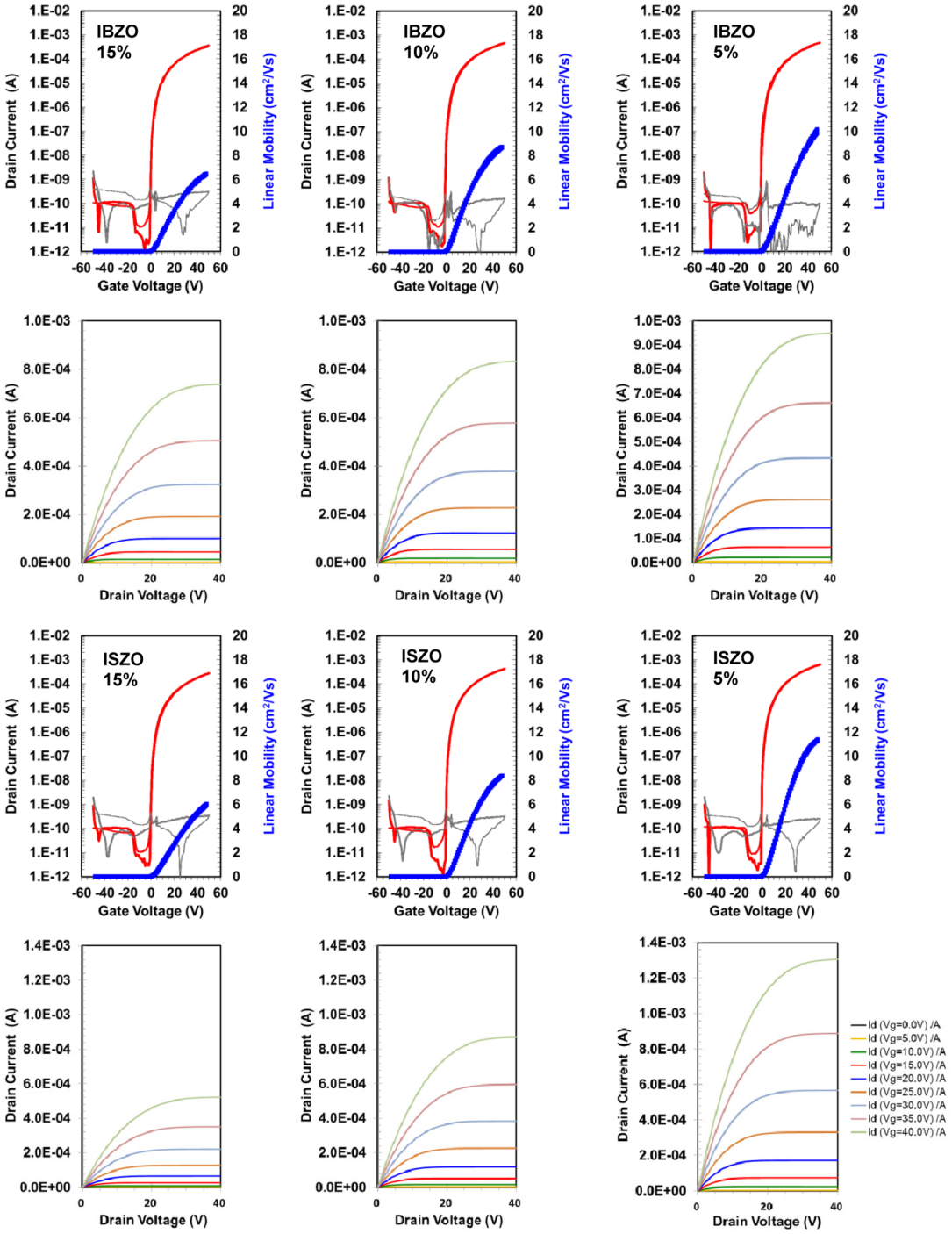

Figure 2. Transfer (drain current vs gate voltage) and output (drain current vs drain voltage) characteristics for bottom−gate, top−contact, solution-processed IBZO (a) and ISZO (b) TFTs (20 nm). All devices were fabricated via spin coating from alkoxide solutions of **1**, **2**, **7**, and **8** on Si/SiO_2 (100 nm) and annealed in air at 450 °C (W = 3000 μm, L = 300 μm, V_{DS} = 5 V).

of Ba (approximately 1.0 atom %) and Cl (2.5 atom %) impurities present, independent of the intentional incorporation of the Ba and Sr precursor dopants. To eliminate the potential influence of these background impurities on device performance we have also used commercially available high purity alkyl metal starting reagents, namely, electronic grade trimethyl indium and diethyl zinc for the synthesis of metal alkoxide derivatives (**4**−**8**).

These metal alkyl reagents have found extensive use in chemical vapor deposition (CVD) or atomic layer deposition (ALD) processes for fabricating III−V and II−VI based semiconducting materials[40] and, more recently, transparent conducting layers (TCO).[3,41] These commercially available reagents are reacted directly with the parent alcohol to achieve the desired metal alkoxide molecular precursor in situ, i.e., $[EtZn(OR')]_4$ and $[(Me)_{3-x}In(OR')_x]_y$, through a simple alcoholysis mechanism (Scheme 1), which we designate as our "ink-on-demand process" due to the facile in situ formation of the metal oxide molecular precursor. In the case of reducing metals such as alkaline earth metals Ba and Sr, in situ reaction with the parent alcohol yields their conjugate alkolate base, and the impurity issue does not arise.

dx.doi.org/10.1021/cm4035837 | *Chem. Mater.* 2014, 26, 1195−1203

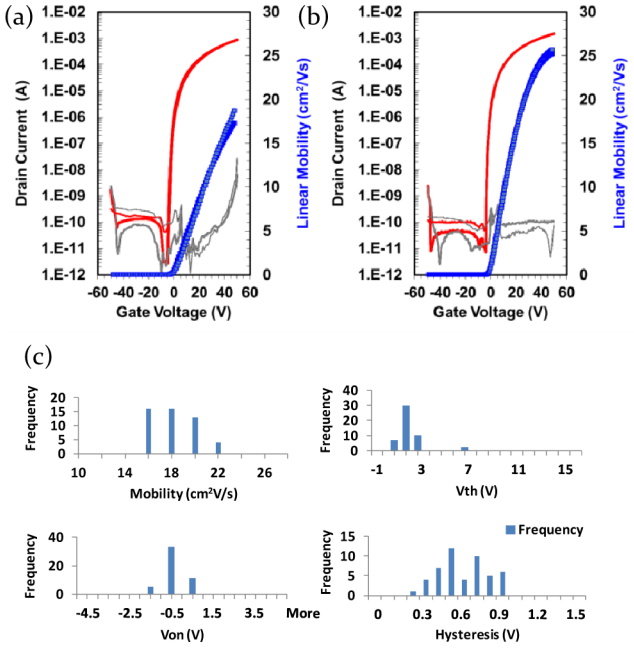

Figure 3. Transfer curve for a BGTC transistor with (a) IBZO and (b) ISZO oxide channel layer fabricated by dipping a 15% doped alkoxide thin film in water for 10 s before air annealing using **1**, **2**, and **7** or **8**. (W/L =10, V_{DS} = 5 V, T = 450 °C). (c) Statistical analysis data for a 7 × 7 array for IBZO 5% doped transistors.

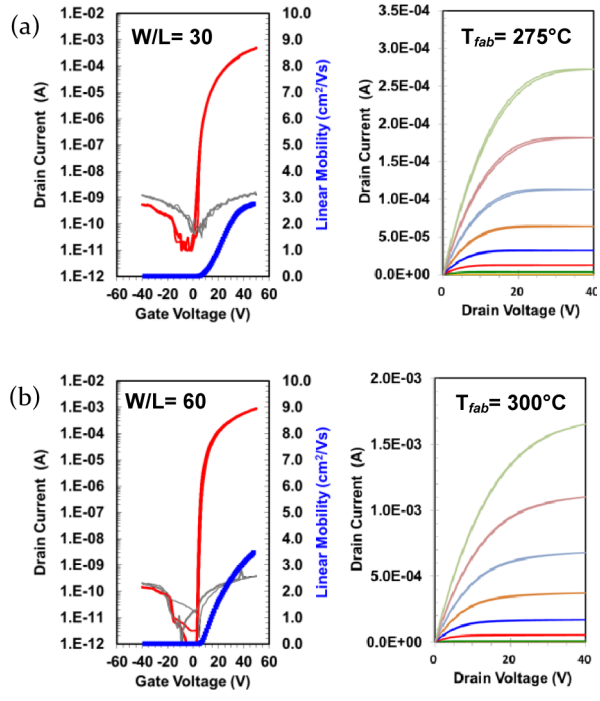

Figure 4. BGTC ISZO TFT devices fabricated at (a) 275 °C and (b) 300 °C, respectively, through hydrolysis via dipping spin coated alkoxide molecular precursor films made from **1**, **2**, and **8** on silicon substrate in deionized water for 10 s before dry annealing at the designated temperatures to afford films with a final doping concentration of 5% (initial doping concentration in the spin-coated films 15%, V_{DS} = 5 V, output curve drain current recorded at V_g = 0−40 V, steps of 5 V).

A clear advantage of this route is the facile in situ formation of the metal alkoxide molecular precursor that permits tailoring

Scheme 1. Preparation of High Purity Molecular Alkoxide Precursors by Alcoholysis Reaction[a]

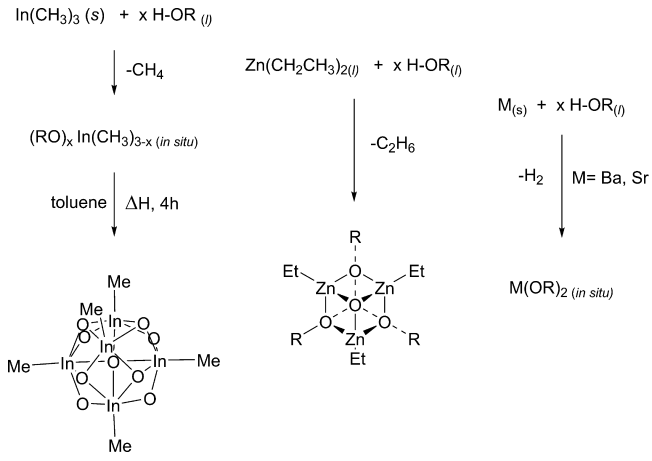

[a]Note: R groups on indium cluster are not shown for clarity.

of the organic ligand through adjustment of the parent alcohol, while also negating the need to isolate the end product, which can often lead to degradation of the reactive alkoxide target compound. By starting with alkyl metal reagents, the only byproducts are eliminated as small alkane molecules or hydrogen gas.

The degree of substitution of the alkoxide ligand for the bound alkyl group on the metal center is known to be dependent on thermodynamics.[42] In the case of alkyl zinc, even with an excess of alcohol present the most thermodynamically stable derivative is found to be the mono substituted $[RZn(OR')]_4$.[43] Attempts to substitute the remaining alkyl group at elevated temperatures have been shown to be possible, however, the end product is a zinc cluster.[43,44] In the case of alkyl indium derivatives both *mono* and *bis* substitution of the bound alkyl group can occur, and the degree of substitution is often directed by the steric hindrance of the residing organic R group, $[R_{3-x}In(OR')_x]$ (where x = 1−2).[29,45,46] Multinuclear NMR analysis of the isolated solids/gels confirms the incorporation of the parent alcohol ligand into the metal alkyl complex [see Supporting Information]. For use in thin film oxide formation, no attempts were made to isolate the final molecular product, but the solutions were used as is. A point to note is that simple metal alkoxide complexes are often insoluble in their parent alcohol. However, with the in situ preparation this was not found to be a problem in our experiments. This is clearly demonstrated in the case of zinc isopropoxide molecular compounds, where the bis substituted derivative is insoluble in the parent alcohol propan-2-ol, and the mono substituted compound is only poorly soluble. However, in situ preparation provides a clear, transparent solution that is stable for 1−2 days before early signs of precipitation are observed. This provides a sufficient window for processing. A further benefit of the "ink-on-demand" process is the ability to tailor the alkoxide ligand by changing the parent alcohol, which can enhance ink stability. This was observed for samples made incorporating the *n*-butoxide ligand. The blended butoxide inks were found to be stable for over 5 days, whereas isopropoxide inks had reduced ink stability of 1−2 days (Figure S6, Supporting Information).

Using the "ink-on-demand" process, IBZO and ISZO films with increasing doping levels of BaO and SrO varying from 5 to 20% were prepared. UV/vis spectroscopic analysis shows that

dx.doi.org/10.1021/cm4035837 | *Chem. Mater.* 2014, 26, 1195−1203

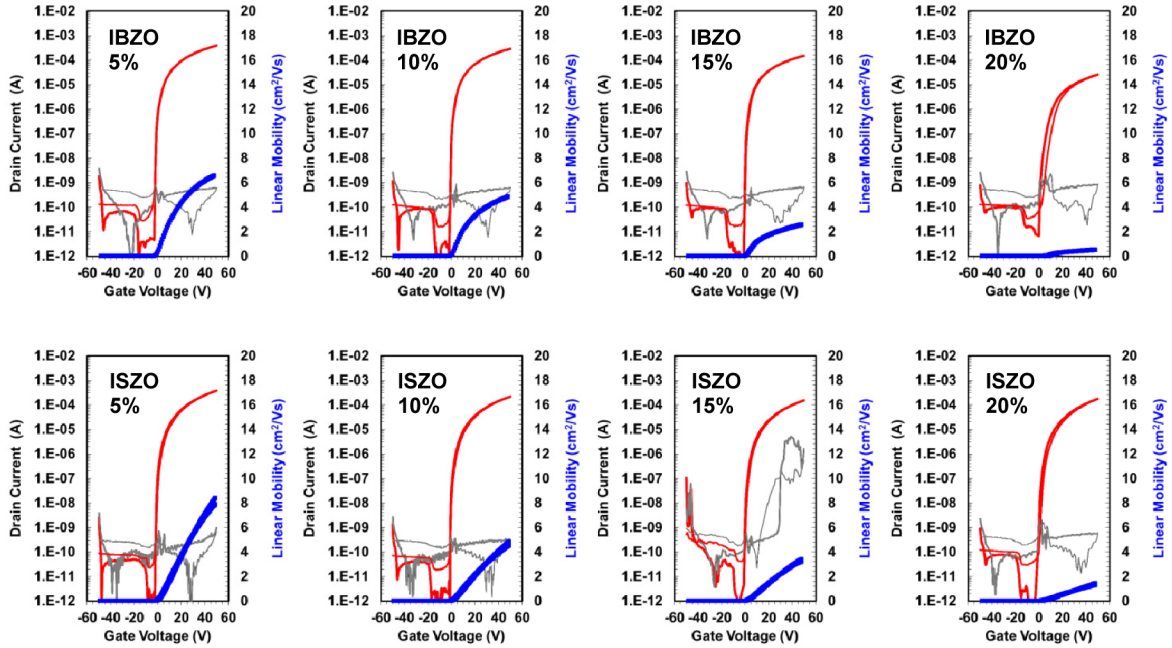

Figure 5. Transfer characteristics for solution processed IBZO and ISZO TFT devices (7:3 In:Zn oxide ratio) made using high-purity molecular precursors **4**, **6**, and **7** or **8** via the "ink-on-demand" process. All devices were annealed at 450 °C for 2 h and have channel width (W) of 3000 μm and lengths (L) 100 or 300 μm (V_{DS} = 5 V). Both forward and reverse curves are recorded.

even at very high doping levels, the films remain transparent, with the band edge showing subtle signs of a red shift as expected due to the incorporation of the wide band gap oxides (Figure S7, Supporting Information). Films also retain their amorphous microstructure as seen in XRD studies on samples with thick, multiple coated oxide layers on silicon or high purity glass. These show no Bragg diffraction peaks (Figure S8, Supporting Information).

AFM studies do however clearly show that incorporating the wide band gap alkaline earth oxide results in an increase in surface roughness of the films (Figures S9 and S10, Supporting Information). This may reflect a greater disorder placed on the metal oxide framework due to the incorporation of the larger cation radii Ba and Sr elements. XPS analysis of the film stoichiometry is in good agreement with the doping concentrations expected from the blending ratio of the molecular precursors (Figure S11, Supporting Information). Additionally, angle resolved XPS analysis, which provides a comparison between surface and bulk properties of the films without the need for sputtering, confirms that the dopants are uniformly distributed throughout the films without apparent surface enrichment or depletion. Only the carbon signal is enhanced on the surface due to inevitable surface contamination (Figure S12, Supporting Information).

TFT devices fabricated using these layers demonstrate excellent characteristics (Figure 5) and mirror the monotonic trend in performance with increased doping concentration that was observed for the lower purity In and Zn precursors made from metal halide starting reagents (Figure 2). The higher doping level acts to suppress carrier concentration, concomitant with a reduction in mobility due to the higher Gibbs energy toward oxidation (Table S3, Figure S13−15, Supporting Information).[47]

The overall observed lower mobility for these devices as shown in Figure 5, in comparison with that when using the indium pentacluster derivative[11] (**1**) (Figure 2), can be attributed to the reported higher degradation temperatures for the simple alkyl indium alkoxides ($[R_{3-x}In(OR')_x]$)[48] (**5**, **6**) than the temperatures for the cluster compound, $In_5O(OCH(CH_3)_2)_{13}$ (**1**).

In order to provide a better comparison we looked at a similar organometallic indium cluster. In a similar way that *tris* substituted indium isopropoxide $[In((OCH(CH_3)_2)_3]$ can afford *coordinated* cluster compounds when subjected to an increase in enthalpy during synthesis,[49] alkyl indium derived alkoxides $[R_{3-x}In(OR')_x]$ have also been shown to afford *organometallic* cluster cage compounds $[(MeIn)_5O(OR)_8]$, which decompose at low temperatures.[45] Inks based on such cluster compounds were also prepared by a similar method to the one first reported by Neumuller et al.[50] and used as is without further isolation or purification (Scheme 1, **9**−**11**). Thus, to now obtain a comparison with the metal halide route to the ink-on-demand route, solution processed IZO TFTs were made using the organometallic indium pentacluster ink $[(MeIn)_5O(OR)_8]$ (**11**) with $[EtZnOCH(CH_3)_2]$ (**4**) and annealed at 450 °C (Figure S16, Supporting Information) and showed excellent performance with high ON/OFF ratios, V_{ON}, low hysteresi,s and with a comparable mobility of 13.8 $cm^2\ V^{-1}\ s^{-1}$.

We thus conclude that device performance is determined by the intrinsic chemical reactivity and properties of the alkoxide functionality and not by the details of precursor synthesis. The similar level of device performance achieved with the high purity ink on demand process shows that the role of the unintentional Ba and halide impurities present in precursors made from halide starting reagents do not exhibit a significant influence on device performance. We note, however, that the two routes differ in their response to processing in water. Our attempts to induce surface hydrolysis of thin alkyl metal alkoxide coatings have not been successful, leaving either discontinuous films or leading to complete film removal. This is

dx.doi.org/10.1021/cm4035837 | *Chem. Mater.* 2014, 26, 1195−1203

most likely due to the presence of the labile metal−carbon bond and thus the highly exothermic reaction with water.

TFT device stability is an important performance parameter which depends critically on the density of electronic defects in the films and at the interface. This is often determined by the shift in threshold voltage (ΔV_{th}) with time upon imposing a prolonged electrical stress such as a constant current or voltage. Continuous bias stress measurements were undertaken using a constant current and voltage for solution-processed ISZO and IBZO TFTs and compared with measurements on IGZO TFTs prepared under directly comparable process conditions. We found that the alkaline earth-doped devices exhibit excellent threshold voltage stability with ΔV_{th} = 1.1 V and 1.4 V for IBZO and ISZO, respectively, after 14 h of continuous stress. In comparison, our IGZO devices displayed an inferior stress stability with ΔV_{th} = 4 V after 14 h of stress. This difference in stability was found to be repeatable across several batches of devices and independent of the starting molecular precursor ink (Figure 6 and Figure S17, Supporting Information). Constant

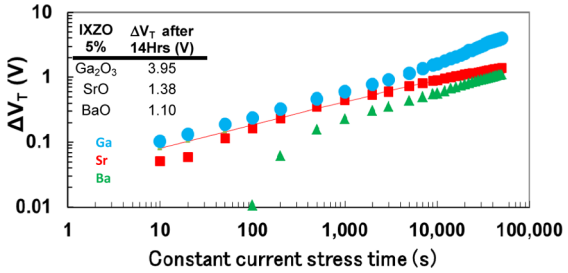

Figure 6. Device Stability: Threshold voltage shift ΔV_{th} as a function of current stress time for IZO TFTs made using **1** and **2** and doped with 5% Ga, Ba, and Sr oxide using **3**, **7**, and **8** annealed at 450 °C. The constant current (10 μA) operational stress was applied at room temperature for approximately 14 h (W/L = 30).

current stress measurements were also evaluated for devices fabricated at reduced temperatures (275 °C) (Figure S18, Supporting Information). The threshold voltage shifts were slightly higher with values of 2.56 and 3.43 V for IBZO and ISZO, respectively, after a constant current stress of 10 μA over 14 h. The temporal dependence shift of the threshold voltage shifts can be described approximately by a stretched exponential law, which suggests that mechanisms for the change in threshold voltage are related to dispersive carrier transport.[51] In each case, transfer curves exhibited a "rigid" shift without significant degradation in mobility and subthreshold slope values (see Supporting Information). Since an increase in subthreshold swing is a key indicator of the presence of shallow sub-gap band states we can conclude the mechanism for the threshold shift is not a result of formation of shallow trap states during stress tests but through the trapping of charges in deep subgap states. This is consistent with the work published by Nomura et al. who reported a detailed study of bias stress stability of IGZO TFTs deposited via sputtering.[52] Using a constant mobility model with the insertion of trap states at 1.0 eV below the conduction band edge, they found an excellent agreement with the threshold voltage shift without degradation of mobility and subthreshold slope. We also note that the devices fully recover after removal of the stress. In terms of the magnitude of the threshold voltage shift, our solution processed TFTs exhibit stability comparable to that of sputtered devices. This suggests that the use of alkaline earth dopants for mixed metal oxides not only is a promising approach for solution processed oxides, but should also be explored for materials deposited by sputtering.

Finally, we have investigated processing approaches for the materials investigated here to further reduce the required annealing temperature and make the process more compatible with low energy budget and low-cost plastic substrates. Recently Kim et al.[53] have shown the use of photoannealing with high intensity UV irradiation under an inert environment for low temperature oxide formation, similar to the original concept investigated by Boyd and Zhang.[54] Pursuant to this we have adapted our methodology to afford TFTs fabricated using a low-medium intensity UV (254 nm) lamp (<10 mW/cm^2). The choice of wavelength negates the need for use in an inert environment since molecular oxygen absorbs at <250 nm. In addition, thermocouples mounted directly on the Si substrates demonstrated that by using low-medium UV intensity no distinct external heating by the UV lamp was observed in our setup (see Experimental Section). High mobility solution spun IBZO and ISZO devices, "cured" via in situ air UV photo annealing, were thus fabricated at maximum anneal temperatures of 200 and 225 °C. TFTs made from thin films subjected to in situ UV annealing using the alkoxide molecular precursors at 225 °C show maximum mobilities of approximately 4 cm^2 V^{-1} s^{-1} for IBZO, Figure 7a. Statistical data analysis for IBZO 49 TFTs yields an average field effect mobility of 3.29 ± 0.64 cm^2 V^{-1} s^{-1}. We note that the lower mobility (2.7−3.0 cm^2 V^{-1} s^{-1}) TFT devices are located near the edges of the spun coated substrate, Figure 7b. Reference TFT devices made in the absence of UV photoannealing were also made, Figure S19 (Supporting Information). Although distinct TFT behavior is recorded for both reference IBZO and ISZO devices, there is a reduction in the drain current and the presence of a large hysteresis between forward and reverse $I-V$ sweeps.

Exploring the boundaries of low temperature processing using the in situ UV process, working TFTs, albeit with reduced mobility and an increase in the hysteresis between forward and reverse IV curves (Figure 7d), were also achievable at a fabrication temperature of 200 °C. However, by reducing the concentration of the wideband gap alkaline oxide from 5% to 2% a near twofold enhancement in mobility from 0.75 to approximately 1.5 cm^2 V^{-1} s^{-1} was achieved.

For these low-temperature processed devices continuous bias stress measurements were undertaken using a constant voltage (+5 V), Figure 7c. Again we found that the alkaline earth-doped devices exhibit excellent threshold voltage stability with ΔV_{th} = 1.36 V and 0.88 V for IBZO and ISZO, respectively, after 14 h of continuous stress. In comparison, our IGZO devices displayed reduced stress stability with ΔV_{th} = 2.69 V after 14 h of stress. Examination of electrical stability for 5% doped IBZO and ISZO devices made at 200 °C also showed remarkable stability with slightly higher threshold voltage shifts of 1.9 and 2.7 V, respectively.

The enhancement of device performance at low annealing temperatures that is achieved by simultaneous UV exposure may be understood in terms of photon absorption by the alkoxide ligands resulting in decomposition of the molecular precursor.[53] However, it has also been noted that for ZnO based systems a reduction in trap states can be achieved by either annealing in a nitrogen atmosphere, UV exposure, or electrical biasing.[55,56] A detailed investigation of the mechanism for the UV assisted lowering of process temperature is underway, but our results clearly demonstrate that alkaline

dx.doi.org/10.1021/cm4035837 | Chem. Mater. 2014, 26, 1195−1203

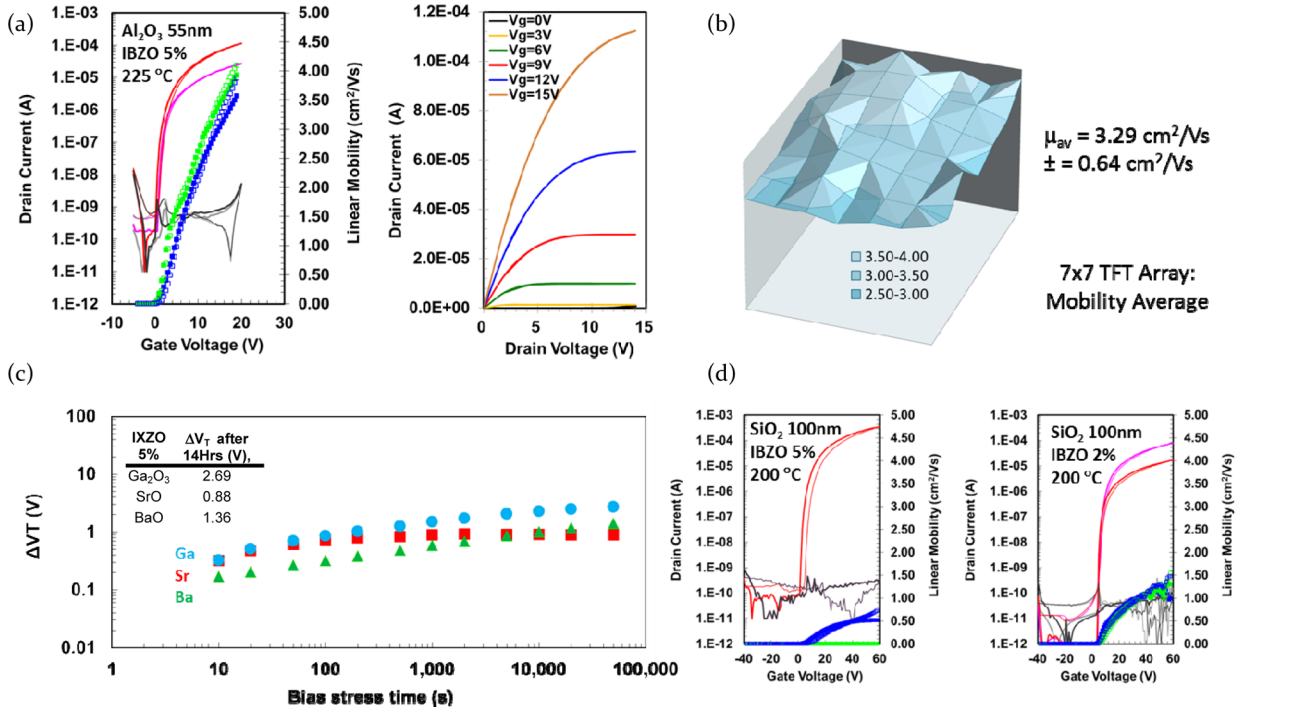

Figure 7. Alkaline earth doped IZO TFTs (VDS 1 and 5 V), made from **1**, **2**, **7**, and **8**: (a) Typical transfer and output curves for solution spun Ba doped IZO (5% oxide), max process temperature of 225 °C, *W* 1000 μm, *L* 200 μm, (b) statistical analysis for 49 TFTs representative of alkaline earth doped devices for IBZO shown in (a), (c) constant voltage electrical bias stress testing (applied bias stress of +5 V over 14 h) for devices fabricated at 225 °C, and (d) IBZO devices fabricated at maximum anneal temperature of 200 °C.

earth doped metal oxides are not only competitive with conventional Ga-doped oxides in terms of performance and stability but are also compatible with state-of-the-art processing methods to achieve low process temperatures around 200−225 °C for these solution-processed materials.

4. CONCLUSION

In summary we have shown that replacing gallium oxide with either barium or strontium oxide affords amorphous, high performance semiconducting oxides with high carrier mobility up to 25 $cm^2\ V^{-1}\ s^{-1}$ and demonstrates for the first time enhanced electrical stability. Alkoxide precursors for these materials can be prepared via a simple "ink-on-demand" process from high purity alkyl metal starting reagents which negate the need for a complex synthetic methodology and purification by utilizing the chemical reactivity of organometallic reagents. The lifetime of the mixed inks can be tailored readily through use of different parent alcohols. We have also shown that these materials are amenable to low temperature processing methods. By dipping the films in water and hydrolyzing the molecular alkoxide precursor coating directly on the substrate prior to annealing at reduced temperatures of 275 °C, we have fabricated TFTs with mobilities of 3−5 $cm^2\ V^{-1}\ s^{-1}$ and excellent stability. By using UV-assisted processing, TFT mobilities of 2−4 $cm^2\ V^{-1}\ s^{-1}$ with excellent stability were achieved at 200−225 °C. Our results demonstrate clearly that solution-processed alkaline earth doped mixed metal oxides provide competitive performance and improved operational stability over conventional Ga-doped materials and are indeed attractive materials for low-temperature solution-processed, high-performance thin film electronics.

■ ASSOCIATED CONTENT

Ⓢ Supporting Information

Materials analysis (XPS, AFM, XRD, and UV/vis), synthetic protocols/methods and NMR analysis, thin film transistor electrical testing, and a doping study for IBZO and ISZO oxide semiconductors is included. This material is available free of charge via the Internet at http://pubs.acs.org.

■ AUTHOR INFORMATION

Corresponding Author

*H.S.: E-mail hs220@cam.ac.uk.

Present Address

‖R.L.P: Electrical and Computer Engineering, EECS Building, 1301 Beal Avenue, Ann Arbor, Michigan 48109-2122, United States.

Author Contributions

⊥K.K.B., R.L.P., K.M., and Y.Y.: All authors contributed equally.

Notes

The authors declare no competing financial interest.

■ ACKNOWLEDGMENTS

This work was supported by a grant from Panasonic Corporation. We also acknowledge financial support from the European Commission through the POINTS project (FP7-NMP-2010-Small-4). We would like to thank Mr. Andrew Wright (Thermo Fisher, Sci., Surface Analysis, East Grinstead, U.K.) for angle resolved XPS analysis.

■ REFERENCES

(1) Barquinha, P. *Transparent oxide electronics: from materials to devices*; Wiley: Hoboken, NJ, 2012.

(2) Facchetti, A.; Marks, T. J. *Transparent electronics: from synthesis to applications*; Wiley: Chichester, UK, 2010.
(3) Ginley, D. S.; Hosono, H.; Paine, D. C. *Handbook of transparent conductors*; Springer: New York, 2010.
(4) Hartnagel, H. *Semiconducting transparent thin films*; Institute of Physics Pub.: Bristol, U.K., Philadelphia, PA, 1995.
(5) Wager, J. F.; Keszler, D. A.; Presley, R. E. *Transparent electronics*; Springer: New York, 2008.
(6) Nomura, K.; Ohta, H.; Takagi, A.; Kamiya, T.; Hirano, M.; Hosono, H. *Nature* **2004**, *432* (7016), 488−492.
(7) Street, R. A. *Adv. Mater.* **2009**, *21* (20), 2007−2022.
(8) Fortunato, E.; Barquinha, P.; Martins, R. *Adv. Mater.* **2012**, *24* (22), 2945−2986.
(9) Kitakado, H.; Katoh, S. *Jpn. J. Appl. Phys.* **2012**, *51* (3), 03CB02-7.
(10) Kim, M. G.; Kanatzidis, M. G.; Facchetti, A.; Marks, T. J. *Nat. Mater.* **2011**, *10* (5), 382−388.
(11) Banger, K. K.; Yamashita, Y.; Mori, K.; Peterson, R. L.; Leedham, T.; Rickard, J.; Sirringhaus, H. *Nat. Mater.* **2011**, *10* (1), 45−50.
(12) Kim, S. J.; Kim, D. L.; Rim, Y. S.; Jeong, W. H.; Kim, D. N.; Yoon, D. H.; Kim, H. J. *J. Cryst. Growth* **2011**, *326* (1), 163−165.
(13) Yoon, D. H.; Kim, S. J.; Jeong, W. H.; Kim, D. L.; Rim, Y. S.; Kim, H. J. *J. Cryst. Growth* **2011**, *326* (1), 171−174.
(14) Kim, G. H. J.; Hee, W.; Ahn, B. D.; Shin, H. S.; Kim, H. J.; Kim, H. J.; Ryu, M.-K.; Park, K.-B.; Seon, J.-B.; Lee, S.-Y. *Appl. Phys. Lett.* **2010**, *96*, 163506.
(15) Kim, D. N.; Kim, D. L.; Kim, G. H.; Kim, S. J.; Rim, Y. S.; Jeong, W. H.; Kim, H. J. *Appl. Phys. Lett.* **2010**, *97*, 192105.
(16) Park, J. C.; Kim, S. W.; Kim, C. J.; Lee, H. N. *IEEE Electron Dev. Lett.* **2012**, *33* (6), 809−811.
(17) Cho, D. H.; Yang, S.; Byun, C.; Ryu, M. K.; Park, S. H. K.; Hwang, C. S.; Yoon, S. M.; Chu, H. Y. *IEEE Electron Dev. Lett.* **2009**, *30* (1), 48−50.
(18) Cho, D. H.; Yang, S.; Park, S. H. K.; Byun, C.; Yoon, S. M.; Lee, J. I.; Hwang, C. S.; Chu, H. Y.; Cho, K. I. *Dig. Tech. Pap. - Soc. Inf. Disp. Int. Symp.* **2009**, 280−283.
(19) Chong, E.; Chun, Y. S.; Lee, S. Y. *Appl. Phys. Lett.* **2010**, *97*, 102102-3.
(20) Kim, C. J.; Kim, S.; Lee, J. H.; Park, J. S.; Kim, S.; Park, J.; Lee, E.; Lee, J.; Park, Y.; Kim, J. H.; Shin, S. T.; Chung, U. I. *Appl. Phys. Lett.* **2009**, *95*, 252103.
(21) Kim, D. H.; Son, D. H.; Sung, S. J.; Kim, J. H.; Kang, J. K. *Mol. Cryst. Liq. Cryst.* **2012**, *564*, 130−137.
(22) Lee, S.; Paine, D. C. *Appl. Phys. Lett.* **2011**, *98*, 262108.
(23) Oh, B. Y.; Park, J. C.; Lee, Y. J.; Cha, S. J.; Kim, J. H.; Kim, K. Y.; Kim, T. W.; Heo, G. S. *J. Solid State Chem.* **2011**, *184* (9), 2462−2465.
(24) Sun, J.; Yang, W. F.; Huang, Y. H.; Lai, W. S.; Lee, A. Y. S.; Wang, C. F.; Gong, H. *J. Appl. Phys.* **2012**, *112*, 083709.
(25) Jeong, W. H. K.; Hee, Gun; Shin, H. S.; Ahn, B. D.; Kim, H. J.; Ryu, M.-K.; Park, K.-B.; Seon, J.-B.; Lee, S. Y. *Appl. Phys. Lett.* **2010**, *96*, 093503.
(26) Chung, Y.-W.; Chen, F.-C.; Chen, Y.-P.; Chen, Y.-Z.; Chueh, Y.-L. *Phys. Status Solidi RRL* **2012**, *6* (9−10), 400−402.
(27) Hennek, J. W.; Smith, J.; Yan, A.; Kim, M. G.; Zhao, W.; Dravid, V. P.; Facchetti, A.; Marks, T. J. *J. Am. Chem. Soc.* **2013**, *135* (29), 10729−41.
(28) Mori, K.; Sirringhaus, H.; Banger, K. K.; Peterson, R. L. Oxide semiconductor. WO2010122274 A1, 2009.
(29) Neumuller, B. *Chem .Soc. Rev.* **2003**, *32* (1), 50−55.
(30) Kamiya, T.; Hosono, H. *NPG Asia Mater.* **2010**, *2* (1), 15−22.
(31) Greenwood, N. N.; Earnshaw, A. *Chemistry of the elements*, 2nd ed.; Butterworth-Heinemann: Oxford; Boston, 1997.
(32) Brinker, C. J.; Scherer, G. W. *Sol-gel science: the physics and chemistry of sol-gel processing*; Academic Press: Boston, 1990.
(33) Jiang, K.; Anderson, J. T.; Hoshino, K.; Li, D.; Wager, J. F.; Keszler, D. A. *Chem. Mater.* **2011**, *23* (4), 945−952.
(34) Aoki, Y.; Kunitake, T.; Nakao, A. *Chem. Mater.* **2005**, *17* (2), 450−458.
(35) Kruger, H. *Chem. Soc. Rev.* **1982**, *11* (3), 227−255.
(36) Livage, J.; Henry, M.; Sanchez, C. *Prog. Solid State Chem.* **1988**, *18* (4), 259−341.
(37) Hwang, Y. H.; Seo, J.-S.; Yun, J. M.; Park, H.; Yang, S. C.; Park, S.-H. K.; Bae, B.-S. *NPG Asia Mater.* **2013**, *5*, e45.
(38) Meyers, S. T.; Anderson, J. T.; Hung, C. M.; Thompson, J.; Wager, J. F.; Keszler, D. A. *J. Am. Chem. Soc.* **2008**, *130* (51), 17603−17609.
(39) Leedham, T. Synthesis of gallium and indium alkoxides. US 20090112012 A1, April 2009.
(40) Jones, A. C.; O'Brien, P. *CVD of compound semiconductors: precursor synthesis, development and applications*; VCH: Weinheim, Germany; Cambridge, 1997.
(41) Knapp, C. E.; Hyett, G.; Parkin, I. P.; Carmalt, C. J. *Chem. Mater.* **2011**, *23* (7), 1719−1726.
(42) Bradley, D. C. *Alkoxo and aryloxo derivatives of metals*; Academic Press: San Diego, 2001.
(43) Steudel, Y.; Steudel, R. *J. Phys. Chem. A* **2010**, *114* (22), 6370−6376.
(44) Kageyama, H.; Miki, K.; Tanaka, N.; Kasai, N.; Ishimori, M.; Heki, T.; Tsuruta, T. *Makromol. Chem., Rapid Commun.* **1982**, *3* (12), 947−951.
(45) Chitsaz, S.; Neumuller, B. *Z. Anorg. Allg. Chem.* **2001**, *627* (11), 2451−2459.
(46) Chitsaz, S.; Iravani, E.; Neumuller, B. *Z. Anorg. Allg. Chem.* **2002**, *628* (11), 2279−2285.
(47) Hosono, H. *J. Non-Cryst. Solids* **2006**, *352* (9−20), 851−858.
(48) Basharat, S.; Carmalt, C. J.; Barnett, S. A.; Tocher, D. A.; Davies, H. O. *Inorg. Chem.* **2007**, *46* (22), 9473−9480.
(49) Bradley, D. C.; Chudzynska, H.; Frigo, D. M.; Hursthouse, M. B.; Mazid, M. A. *J. Chem. Soc., Chem. Commun.* **1988**, *18*, 1258−1259.
(50) Chamazi, N. N.; Heravi, M. M.; Neumuller, B. *Z. Anorg. Allg. Chem.* **2006**, *632* (12−13), 2043−2048.
(51) Nomura, K.; Kamiya, T.; Kikuchi, Y.; Hirano, M.; Hosono, H. *Thin Solid Films* **2010**, *518* (11), 3012−3016.
(52) Nomura, K.; Kamiya, T.; Hirano, M.; Hosono, H. *Appl. Phys. Lett.* **2009**, *95*, 013502.
(53) Kim, Y. H.; Heo, J. S.; Kim, T. H.; Park, S.; Yoon, M. H.; Kim, J.; Oh, M. S.; Yi, G. R.; Noh, Y. Y.; Park, S. K. *Nature* **2012**, *489* (7414), 128−U191.
(54) Boyd, I. W.; Zhang, J. Y. *Solid-State Electron.* **2001**, *45* (8), 1413−1431.
(55) Lin, Y.-H.; Faber, H.; Rossbauer, S.; Anthopoulos, T. D. *Appl. Phys. Lett.* **2013**, *102*, 193516.
(56) Small, C. E.; Chen, S.; Subbiah, J.; Amb, C. M.; Tsang, S. W.; Lai, T. H.; Reynolds, J. R.; So, F. *Nat. Photonics* **2012**, *6* (2), 115−120.